J|A|C|S
COMMUNICATIONS

Published on Web 12/09/2006

The Two-State Issue in the Mixed-Valence Binuclear Cu_A Center in Cytochrome *c* Oxidase and N_2O Reductase

Serge I. Gorelsky,[†] Xiangjin Xie,[†] Ying Chen,[‡] James A. Fee,[‡] and Edward I. Solomon*,[†]

Department of Chemistry, Stanford University, 333 Campus Drive, Stanford, California 94305, and Division of Biology, The Scripps Research Institute, La Jolla, California 92037

Received October 23, 2006; E-mail: edward.solomon@stanford.edu

The binuclear Cu_A site found both in cytochrome *c* oxidase (C*c*O)[1] and nitrous oxide reductase (N_2OR)[2] functions in long-range electron transfer (ET). Studies of Cu_A sites have been facilitated by the construction of inorganic models[3] and the perturbation of Cu_A sites by mutation[4] and by inserting Cu_A into proteins containing cupredoxin folds.[5,6] The Cu_A site is defined as a $Cu_2(S_{Cys})_2$ cluster (Figure 1A) with a short Cu−Cu distance (EXAFS $d_{Cu-Cu} = 2.43-2.44$ Å);[7,8] the Cu_2S_2 atoms are nearly planar and each copper ion is further coordinated equatorially by N_{His} and axially by either S_{Met} or carbonyl O.[1,2,9]

In its oxidized state, Cu_A is a delocalized (class III) mixed-valence species $Cu^{1.5+}Cu^{1.5+}$.[10−13] The ground-state (GS) wave function, quantified by X-ray absorption spectroscopy (XAS), is highly covalent,[13] with the spin density delocalized over the Cu_2S_2 cluster. This greatly contributes to the redox properties by lowering the reorganization energy and providing superexchange hole coupling for long-range ET into and out of the Cu_A center. From studies of a model complex ($d_{Cu-Cu} = 2.92$ Å)[3] relevant to the Cu_A protein site, there are two types of GS wave function, σ_u* and π_u (Figure 1B), which interchange depending on the Cu−Cu distance (σ_u* for Cu_A at a short d_{Cu-Cu} and π_u for the model complex at a long d_{Cu-Cu}).[12] Density-functional theory (DFT) calculations of the Cu_A site reveal that the GS potential energy surface of the mixed-valence, oxidized cluster is flat with two minima,[14] which correspond to the σ_u* ($d_{Cu-Cu} = 2.49$ Å, Figure 1A) and π_u ($d_{Cu-Cu} = 3.06$ Å, Figure 1B) electronic states.

As first discussed by Neese and co-workers,[15−17] π_u is the lowest excited-state for the Cu_A site in the protein but its energy has been controversial. EPR data on Cu_A proteins show a low $g_{||}$ value of 2.19 (Table S1) which derives from spin-orbital coupling between the σ_u* GS and the π_u excited-state which requires an energy gap of 3000−4500 cm^{-1}.[12,15] On the other hand, from paramagnetic NMR studies, it has been observed that the lowest-energy excited-state is thermally accessible and the energy gap between the GS and the thermally accessible state is ∼350 cm^{-1}.[18] This has been found in the Cu_A site from *P. verstus* and *P. denitrificans*, which have the same spectral features in UV−vis absorption and equivalent EPR *g*-values (Table S1). This study addresses this apparent discrepancy and evaluates the possible role of the two electronic states, σ_u* and π_u, in ET of Cu_A.

UV−vis absorption of Cu_A from *Thermus thermophilus* (*Tt*) is given in Figure 2A which is similar to other Cu_A sites, and its EPR *g*-values are also equivalent to the other Cu_A sites (Table S1). The $g_{||}$ of 2.19 can be used through eq 1[15] to estimate the energy (Δ) of the π_u excited-state relative to the σ_u* GS of Cu_A. α^2 is the total Cu character in the σ_u* GS which is 44% from Cu L-edge XAS.[13] The Cu character in the π_u excited-state, β^2 is 31% (Table S2) from the DFT calculations below. These give a σ_u*−π_u energy gap

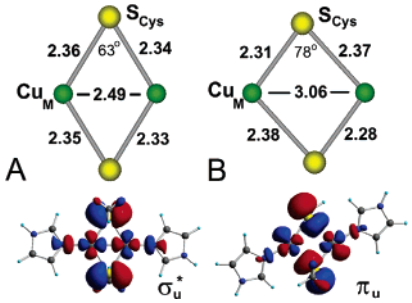

Figure 1. (top) DFT-optimized ground state structures of Cu_A without the protein environment: (A) σ_u* state and (B) π_u state (only Cu_2S_2 cluster is shown for simplicity, internuclear distances are given in Å, Cu_M denotes the Cu atom with the axial Met ligand); (bottom) β-spin LUMO (contour value = 0.03 a.u.) of the $[Cu_2(SCH_3)_2(imz)_2]^+$ complex (Figure S1a) in the (A) σ_u* and (B) π_u ground states.

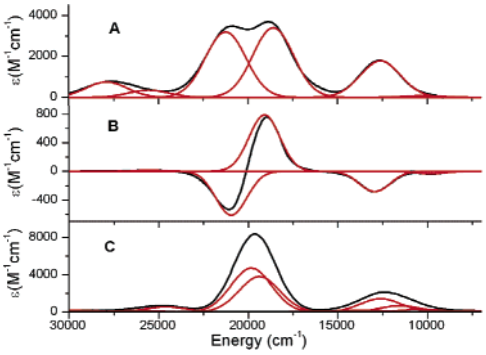

Figure 2. (A) Room-temperature absorption; (B) low-temperature (5 K) MCD spectra of *Tt* Cu_A; (C) TDDFT calculated absorption spectrum of the Cu_A model (total absorption, black; individual components, red).

of ∼5000 cm^{-1} (Table S1). Paramagnetic NMR behavior of *Tt* Cu_A is similar to the other Cu_A proteins (Table S1) indicating a presence of the thermally accessible state within the energy range estimated for the other Cu_A proteins (∼450 cm^{-1}).

$$g_{||} = g_e + \frac{8\zeta_{3d}^{Cu}\alpha^2\beta^2}{\Delta} \qquad (1)$$

The MCD spectrum (Figure 2B) can be used to resolve individual electronic transitions (Figure 2A, red lines) in the absorption spectrum of Cu_A. Time-dependent DFT (TDDFT) (Figure 2C) on Cu_A (see Supporting Information for details) reproduces the experimental absorption spectrum well and gives the parity-forbidden, lowest-energy excited-state π_u at 3200 cm^{-1} above the σ_u* GS. This result is consistent with the EPR-derived energy gap. However, the thermally accessible excited-state is not revealed in TDDFT calculations in the Cu_A geometry.

We can use TDDFT calculations supported by the spectroscopic data on Cu_A to map the GS and excited-state potential energy

[†] Stanford University.
[‡] The Scripps Research Institute.

10.1021/ja067583i CCC: $33.50

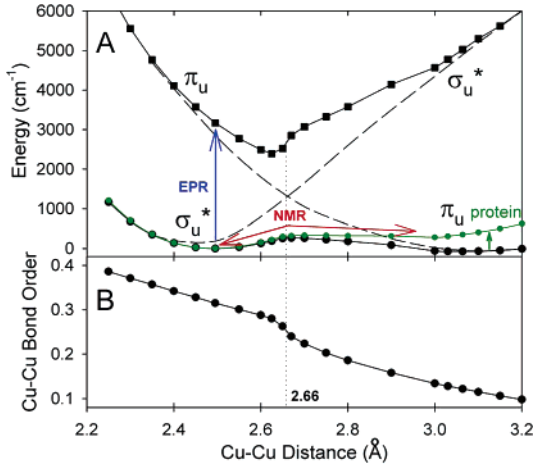

Figure 3. (A) The ground state and the first excited-state potential energy surfaces (black lines, Cu_A cluster in the vacuum; green, the cluster in the protein environment) and (B) Mayer bond order between the two Cu atoms in the GS of Cu_A as a function of the Cu−Cu distance.

surfaces (PES). These calculations (Figure 3A) reveal the electronic coupling between the σ_u* and π_u states which is a function of the Cu−Cu distance. The crossing point between the two states is at $d_{Cu-Cu} = 2.66$ Å and coincides with the inflection point of the Cu−Cu bond order[19] curve (Figure 3B).

These PES calculations show that both NMR and EPR results are consistent with the electronic/geometric structure of Cu_A. The anti-Curie behavior observed in paramagnetic NMR studies of Cu_A results from the thermal equilibrium between the σ_u* and π_u GSs which are at very close energies in their respective equilibrium geometries (Figure 3A). Alternatively, the EPR *g*-value analysis involves the σ_u* GS in the geometry with a short d_{Cu-Cu} where the π_u is a Frank−Condon excited-state calculated to be at 3200 cm^{-1}.

Similar energies but different wave functions of the σ_u* and π_u GS of Cu_A suggest different chemical bonding in the two states. Going from the σ_u* GS with the short Cu−Cu internuclear distance to π_u, the Cu−Cu bond order decreases from 0.32 to 0.12 (Figure 3B), indicating a significant decrease of the direct Cu−Cu bonding interaction. However, the sum of the Cu−S and Cu−Cu bond orders (Figure S3) has decreased only slightly in the two states, thus the loss of the Cu−Cu interaction is compensated by (1) the gain in Cu−S interactions and (2) a reduction of the electronic exchange repulsion in the π_u GS relative to the σ_u* GS (Table S3). Thus the electronic energies of the σ_u* GS and the π_u GS remain very close.

In the π_u GS of Cu_A, the Cu−S_{Cys} covalency becomes localized resulting in two short and two long Cu−S_{Cys} bonds (Figure 1B). The decreased Cu−Cu interaction (Figure 3B) results in a spin distribution in the Cu_A cluster that is easier to localize under the low-symmetry ligand-field of metal axial ligand (Figure S4) and electrostatic perturbations in the protein environment (Table S2). Localization of the Cu−S covalency and valence-trapping lead to larger inner- and outersphere reorganization energies (λ_i and λ_o) of the π_u GS relative to the σ_u* GS (Table S4). The calculated λ_i of the π_u GS is 1.6 times higher than λ_i of the σ_u* GS.

Since the σ_u* and π_u GSs of Cu_A have very similar energies, the ET driving force changes by only ~43 mV in going from the σ_u* GS to the π_u GS. Thus, the factors that can influence the ET rate between Cu_A and its redox partners are the donor−acceptor electronic coupling and the reorganization energies. Using Marcus theory it is possible to evaluate relative efficiency, k_σ/k_π, of the two states for ET. The calculated ET rate ratios in the heme *c* → Cu_A and Cu_A → heme *a* pathways (Figure S5) are ~15 for both of these processes which suggests that the π_u GS is much less efficient for long-range ET than the σ_u* state.

DFT calculations of the Cu_A site without the protein environment (Figure S1a,b) result in the π_u GS being a slightly lower-energy state relative to the σ_u* GS (Figure 3A). Expanding the QM calculations from the 51-atom Cu_A site model (Figure S1b) to 217 atoms (Figure S1c**)** or all protein atoms (using the QM/MM method) results in the σ_u* GS of Cu_A as the lowest-energy state with a d_{Cu-Cu} of 2.44 Å (Figure 3A, green line) in agreement with the EXAFS data (d_{Cu-Cu} = 2.43−2.44 Å).[8] This relative stability derives from the fact that the noncovalent interactions, including H-bonds between the protein backbone amides and the S_{Cys} atoms of the Cu_A site, stabilize the σ_u* GS (which has less spin density and more negative charge on the S_{Cys} atoms, Table S2) relative to the π_u GS. Thus, the protein environment plays a role in maintaining Cu_A in the σ_u* as a lowest-energy state with the lowest reorganization energy for efficient intra- and intermolecular ET with a low-driving force.

Acknowledgment. This research was supported by NSF Grant CHE 0446304 (E.I.S.) and NIH Grants DK31450 (E.I.S.) and GM35342 (J.A.F.). S.I.G. thanks NSERC (Ottawa) for a postdoctoral fellowship.

Supporting Information Available: Experimental details of *Tt* Cu_A, the description of the QM models, and the results of these calculations. This material is available free of charge via the Internet at http://pubs.acs.org.

References

(1) Iwata, S.; Ostermeier, C.; Ludig, B.; Michel, H. *Nature* **1995**, *376*, 660.
(2) Brown, K.; Djinovic-Carugo, K.; Haltia, T.; Cabrito, I.; Saraste, M.; Moura, J. J. G.; Moura, I.; Tegoni, M.; Cambillau, C. *J. Biol. Chem.* **2000**, *275*, 41133.
(3) Houser, R. P.; Young, V. G.; Tolman, W. B. *J. Am. Chem. Soc.* **1996**, *118*, 2101.
(4) Zumft, W. G.; Viebrocksambale, A.; Braun, C. *Eur. J. Biochem.* **1990**, *192*, 591.
(5) Hay, M.; Richards, J. H.; Lu, Y. *Proc. Nat. Acad. Sci. U.S.A.* **1996**, *93*, 461.
(6) Dennison, C.; Vijgenboom, E.; Devries, S.; Vanderoost, J.; Canters, G. W. *FEBS Lett.* **1995**, *365*, 92.
(7) Blackburn, N. J.; Barr, M. E.; Woodruff, W. H.; Vanderooost, J.; Devries, S. *Biochemistry* **1994**, *33*, 10401.
(8) Blackburn, N. J.; de Vries, S.; Barr, M. E.; Houser, R. P.; Tolman, W. B.; Sanders, D.; Fee, J. A. *J. Am. Chem. Soc.* **1997**, *119*, 6135.
(9) Haltia, T.; Brown, K.; Tegoni, M.; Cambillau, C.; Saraste, M.; Mattila, K.; Djinovic-Carugo, K. *Biochem. J.* **2003**, *369*, 77.
(10) Kroneck, P.; Antholine, W.; Riester, J.; Zumft, W. *FEBS Lett.* **1988**, *242*, 70.
(11) Kroneck, P. M. H.; Antholine, W. E.; Riester, J.; Zumft, W. G. *FEBS Lett.* **1989**, *248*.
(12) Gamelin, D. R.; Randall, D. W.; Hay, M. T.; Houser, R. P.; Mulder, T. C.; Canters, G. W.; de Vries, S.; Tolman, W. B.; Lu, Y.; Solomon, E. I. *J. Am. Chem. Soc.* **1998**, *120*, 5246.
(13) DeBeer George S.; Metz, M.; Szilagyi, R. K.; Wang, H. X.; Cramer, S. P.; Lu, Y.; Tolman, W. B.; Hedman, B.; Hodgson, K. O.; Solomon, E. I. *J. Am. Chem. Soc.* **2001**, *123*, 5757.
(14) Olsson, M. H. M.; Ryde, U. *J. Am. Chem. Soc.* **2001**, *123*, 7866.
(15) Neese, F.; Zumft, W.; Antholine, W.; Kroneck, P. M. H. *J. Am. Chem. Soc.* **1996**, *118*, 8692.
(16) Farrar, J. A.; Neese, F.; Lappalainen, P.; Kroneck, P. M. H.; Saraste, M.; Zumft, W. G.; Thomson, A. J. *J. Am. Chem. Soc.* **1996**, *118*, 11501.
(17) Neese, F.; Kappl, R.; Hottermann, J.; Zumft, W. G.; Kroneck, P. M. H. *J. Biol. Inorg. Chem.* **1998**, *3*, 53.
(18) Salgado, J.; Warmerdam, G.; Bubacco, L.; Canters, G. W. *Biochemistry* **1998**, *37*, 7378.
(19) Mayer, I. *Chem. Phys. Lett.* **1983**, *97*, 270.

JA067583I